A common brain network links development, aging, and vulnerability to disease

Gwenaëlle Douaud[a,1], Adrian R. Groves[a], Christian K. Tamnes[b], Lars Tjelta Westlye[c,d], Eugene P. Duff[a], Andreas Engvig[b], Kristine B. Walhovd[b], Anthony James[e], Achim Gass[f], Andreas U. Monsch[g], Paul M. Matthews[h], Anders M. Fjell[b], Stephen M. Smith[a], and Heidi Johansen-Berg[a]

[a]Functional Magnetic Resonance Imaging of the Brain (FMRIB) Centre, Nuffield Department of Clinical Neurosciences, University of Oxford, John Radcliffe Hospital, Oxford OX3 9DU, United Kingdom; [b]Research Group for Life-Span Changes in Brain and Cognition, Department of Psychology and [c]Department of Psychology, University of Oslo, 0317 Oslo, Norway; [d]Norwegian Centre for Mental Disorders Research (NORMENT), KG Jebsen Centre for Psychosis Research, Division of Mental Health and Addiction, Oslo University Hospital, 0424 Oslo, Norway; [e]Department of Psychiatry, University of Oxford, Oxford OX3 7JX, United Kingdom; [f]Department of Neurology, University Hospital Mannheim, University of Heidelberg, 68167 Heidelberg, Germany; [g]Memory Clinic, University Center for Medicine of Aging Basel, Felix Platter-Hospital, CH-4031 Basel, Switzerland; and [h]Division of Brain Sciences, Department of Medicine, Imperial College London, London W12 0NN, United Kingdom

Edited by Denise C. Park, University of Texas at Dallas, Dallas, TX and accepted by the Editorial Board October 15, 2014 (received for review June 4, 2014)

Several theories link processes of development and aging in humans. In neuroscience, one model posits for instance that healthy age-related brain degeneration mirrors development, with the areas of the brain thought to develop later also degenerating earlier. However, intrinsic evidence for such a link between healthy aging and development in brain structure remains elusive. Here, we show that a data-driven analysis of brain structural variation across 484 healthy participants (8–85 y) reveals a largely—but not only—transmodal network whose lifespan pattern of age-related change intrinsically supports this model of mirroring development and aging. We further demonstrate that this network of brain regions, which develops relatively late during adolescence and shows accelerated degeneration in old age compared with the rest of the brain, characterizes areas of heightened vulnerability to unhealthy developmental and aging processes, as exemplified by schizophrenia and Alzheimer's disease, respectively. Specifically, this network, while derived solely from healthy subjects, spatially recapitulates the pattern of brain abnormalities observed in both schizophrenia and Alzheimer's disease. This network is further associated in our large-scale healthy population with intellectual ability and episodic memory, whose impairment contributes to key symptoms of schizophrenia and Alzheimer's disease. Taken together, our results suggest that the common spatial pattern of abnormalities observed in these two disorders, which emerge at opposite ends of the life spectrum, might be influenced by the timing of their separate and distinct pathological processes in disrupting healthy cerebral development and aging, respectively.

brain structure | development | aging | schizophrenia | Alzheimer's disease

Many phylogenetic or ontogenetic models attempt to relate development and aging at genetic, molecular, or cognitive systems levels (1–4). In neuroscience, one of the most popular hypotheses in this respect postulates that the process of healthy age-related brain decline mirrors developmental maturation. This concept was first introduced in 1881 as a "loi de régression" (Ribot's law) when Théodule Ribot, a French philosopher, observed that the destruction of memories progresses in reverse order to that of their formation: from the unstable to the stable, from the newly formed memories to older "sensory, instinctive" memories (5). More generally, this hypothesis postulates that the sequence of events associated with brain decline should present itself in reverse order to the series of events related to brain development, with brain regions thought to develop relatively late—at both ontogenetic and phylogenetic levels—also degenerating relatively early (2, 6, 7).

One way of tracking this hypothesized mirroring pattern of development and aging in the human brain is to use the information provided at a macroscopic level by structural MRI in large-scale, lifespan human populations. Although structural MRI does not distinguish between the various cellular mechanisms underpinning development and aging processes [e.g., dendritic and synaptic remodeling, neurogenesis and neuronal death, astrogliosis, (de)myelination], this technique is sensitive to detect the overall contribution of these mechanisms to macroscopic age-related changes in brain structure (8–10).

In 2000, Raz (11) presented for the first time MRI data suggesting that the chronological order of completion of intracortical fibers myelination was associated with age-related differences in cortical volume. In particular, Raz (12) later noted that "the pattern of differential brain aging suggests that phylogenetically newer and ontogenetically less precocious brain structures such as association cortices and the neostriatum show increased vulnerability to the effects of aging … follow(ing) the rule of (phylogenetically and ontogenetically) last-in, first-out" (12). Direct and intrinsic evidence for a clear link between brain structural development and aging lending support to this evolutionary–developmental "retrogenesis" model [or the "last-in, first-out" model as Raz (12) and others call it] is needed, however. Most of

Significance

Many evolutionary–developmental models have attempted to relate development and aging, with one popular hypothesis proposing that healthy age-related brain decline mirrors developmental maturation. But this elegant hypothesis has so far lacked clear and direct data to support it. Here, we describe intrinsic, entirely data-driven evidence that healthy brain degeneration and developmental process mirror one another in certain brain regions. Specifically, a data-driven decomposition of structural brain images in 484 healthy participants reveals a network of mainly higher-order regions that develop relatively late during adolescence, demonstrate accelerated degeneration in old age, and show heightened vulnerability to disorders that impact on brain structure during adolescence and aging. These results provide a fundamental link between development, aging, and disease processes in the brain.

Author contributions: G.D., E.P.D., S.M.S., and H.J.-B. designed research; G.D., C.K.T., L.T.W., A.E., K.B.W., A.J., A.G., A.U.M., P.M.M., and A.M.F. performed research; A.R.G., E.P.D., and S.M.S. contributed new reagents/analytic tools; G.D., A.R.G., and L.T.W. analyzed data; and G.D. wrote the paper.

The authors declare no conflict of interest.

This article is a PNAS Direct Submission. D.C.P. is a guest editor invited by the Editorial Board.

Freely available online through the PNAS open access option.

Data deposition: The *Z*/*t* stats 3D maps for all three datasets reported in this paper can be found at www.fmrib.ox.ac.uk/analysis/LIFO+AD+AOS/.

[1]To whom correspondence should be addressed. Email: douaud@fmrib.ox.ac.uk.

This article contains supporting information online at www.pnas.org/lookup/suppl/doi:10.1073/pnas.1410378111/-/DCSupplemental.

the structural imaging studies investigating relationships between development and aging have so far led to different, and sometimes contradictory, results (13, 14). One possible explanation for this inconsistency is that these studies have tested only one specific pattern of age-related change and have focused on age subgroups or on predefined regions of the brain.

Here, we took a purely data-driven approach to assess the intersubject brain structure variability among 484 healthy participants covering most of the lifespan (8–85 y). We analyzed the structural brain images of these healthy subjects using a linked independent component analysis (ICA) (*SI Materials and Methods*) (15). This approach provides an automatic decomposition of the images into spatial components characterizing the intersubject brain structural variability, i.e., each spatial component represents a mode of variation of brain structure across all participants.

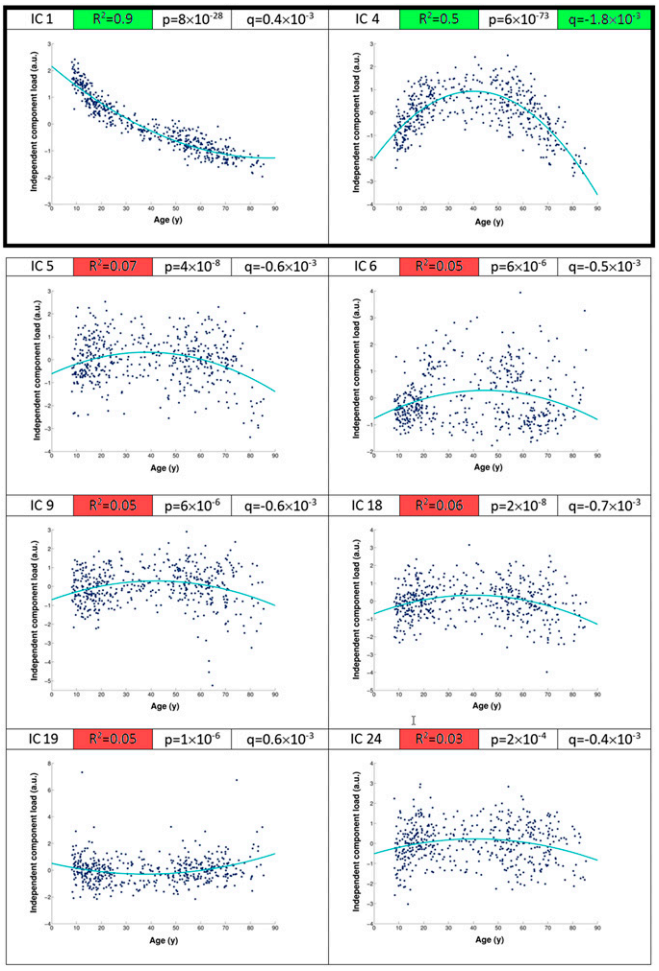

Fig. 1. Of all eight age-related components, only two achieved clear practical significance. We assessed post hoc the relationship of each of the 70 components with age (using polynomial fit). Of eight statistically significant components (all $P < 0.05$ corrected for multiple comparisons), only two achieved clear practical significance (IC1 and IC4), as measured by the percentage of age-related variance explained with a quadratic fit (indicated by the R^2 values): the "global" dominant mode showing monotonic decrease of the whole gray matter with age (IC1), with 90% of the variance of IC1 across subjects explained by age ($R^2 = 0.9$), and the inverted-U component (IC4), with 50% of IC4 variance explained by age ($R^2 = 0.5$). R^2 values for all other components were below 0.1. The inverted-U component IC4 showed a symmetric, strong nonmonotonic relationship with age and presented the strongest quadratic fit as measured by its quadratic coefficient ($q = -1.8 \times 10^{-3}$). a.u., arbitrary unit.

Results

We obtained 70 independent components from this unbiased decomposition that was solely based on the structural information in the gray matter images. As the ICA is, thus, blind to any of the participants' demographics or cognitive measures, we identified post hoc two components that showed strong statistical, as well as practical, association with age (i.e., significance was measured here using effect magnitude in addition to corrected *P* values) (Fig. 1). The first independent component (IC1) represented the expected dominant mode of variation showing the monotonic decrease of the whole gray matter with increasing age typically reported in large-scale lifespan studies (16). Spatially, it essentially described the standard deviation across all gray matter images (explaining ∼50% of the structural variance across participants) (*SI Materials and Methods*), and post hoc analysis revealed that age explained 90% of IC1 variance.

Critically, our data-driven approach made it possible to identify a distinct second age-related component (IC4) accounting for a more subtle part of the structural variance, and showing a nonmonotonic post hoc relationship with age. It defined a spatially specific network of mainly transmodal regions encompassing heteromodal cortex, and limbic and paralimbic regions (17): lateral prefrontal cortex, frontal eye field, intraparietal sulcus, superior temporal sulcus, posterior cingulate cortex, and medial temporal lobe (Fig. 2, Fig. S1, and Table S1). Additional regions included the parietal operculum (especially OP1), crus of the cerebellum, fusiform and lingual gyrus, supplementary motor area (SMA), and a focal, lateral portion of the primary motor cortex (M1). Post hoc analysis revealed that this independent component IC4 had a striking inverted-U relationship with age peaking at 40 y (Figs. 1 and 2 and *SI Materials and Methods*). While this component accounted for 3% of the structural variance across all 484 participants, it had a strong relationship with age, as age explained 50% of the variance within the IC4 component (Fig. S2).

Broadly speaking, each component of an ICA describes a mode of variation—here, specifically, a mode of variation of brain structure—over and above variation associated with all other components. Each voxel of the structural image for every participant can be seen as the sum of each of these components for that same voxel, weighted by the amount of structural variance that they explain. Therefore, in the regions defined by the second age-related component IC4, the variation in brain structure across subjects is explained by the additional effect of this symmetric inverted-U shape on top of the dominant mode of strong monotonic decrease of the whole gray matter with age seen in IC1 (Fig. 3). This inverted-U component IC4 thus describes a network of regions which, compared with the rest of the gray matter, develop relatively late and slowly during adolescence and young adulthood, but show accelerated age-related degeneration in old age (Fig. 3).

This brain network, characterized at one end of the life spectrum by healthy late development and at the other end by healthy accelerated degeneration, might therefore show particular vulnerability to disorders that impact on brain structure during adolescence (18) and aging (19), regardless of their etiology. To test this hypothesis, we used structural imaging data from a study of Alzheimer's disease and a study of adolescent-onset schizophrenia, two diseases that serve here as models of unhealthy aging and development, respectively, to compare their spatial pattern of structural vulnerability with the inverted-U spatial network of IC4. It should be noted at this stage that this hypothesis does not suppose that these disorders should have common pathological processes causing brain structural damage. What we are interested in here is whether the timing of such distinct pathologies in disrupting normal brain development and aging, at a time when regions of the inverted-U network are experiencing the greatest change, leads to similar patterns of structural damage in this network. We found that the spatial distribution of this inverted-U component IC4 not only closely matched the gray matter regions which show accelerated atrophy in Alzheimer's disease ($r = 0.55$,

$P < 10^{-3}$) (Fig. 4, *SI Materials and Methods*, and Figs. S1 and S3), but also matched those regions showing an altered developmental trajectory in adolescent-onset schizophrenia ($r = 0.48$, $P < 10^{-3}$) (Fig. 5). Direct comparison of the spatial distribution between Alzheimer's disease and adolescent-onset schizophrenia pattern of macrostructural abnormalities also revealed a good spatial cross-correlation ($r = 0.48$, $P < 10^{-3}$) (Fig. S3).

Of all 70 components, this close resemblance to both schizophrenia and Alzheimer's disease spatial patterns was only specific to the inverted-U mode of variation IC4 and the dominant mode of variation IC1, as the latter simply represents the standard deviation across all subjects (Fig. S2). Although the inverted-U component was purely derived from healthy individuals, discrimination analysis using this spatial network also allowed for good separation of brain scans between patients with either Alzheimer's disease or schizophrenia and corresponding matched controls (72% and 83% accuracy, respectively) (*SI Materials and Methods*).

The inverted-U component IC4 also differed between males and females (Fig. S4). Females showed a significantly higher and slightly later peak with age than males (41 versus 39 y, respectively; $P = 4.5 \times 10^{-3}$) (*SI Materials and Methods*). This few years of difference in lifespan trajectory of a relevant brain structural component could be related to the later age of onset of symptoms observed in females with schizophrenia and Alzheimer's disease (20, 21).

Finally, additional regression analyses in the large-scale lifespan healthy population showed specific, strong correlations between the strength of the inverted-U component IC4 and episodic memory and intellectual ability, deficits in which are hallmarks of Alzheimer's disease and schizophrenia, respectively ($P << 10^{-3}$) (*SI Materials and Methods*). More specifically, there was a moderate correlation of $r = 0.31$ between the network strength and long-delay free recall on the California Verbal Learning Test (CVLT), which is known to be the most salient measure of memory deficit in mild cognitive impairment and Alzheimer's disease (Fig. 4) (22). There was also a good correlation of $r = 0.40$ between the network strength and fluid intelligence (block design; Wechsler Abbreviated Scale of Intelligence, WASI) (Fig. 5). We found a more modest correlation of $r = 0.21$ between the network strength and crystallized intelligence (vocabulary; WASI) (Fig. S5). However, when looking at the same relationship only in the healthy participants under 40 y old (age peak of the inverted-U component), we found a very strong correlation of $r = 0.52$, consistent with the notion that verbal intelligence crystallizes to a plateau in middle age (Figs. S5 and S6).

Discussion

Here, a data-driven analysis of brain structural variation across 484 healthy participants revealed a previously unseen component showing a symmetric inverted-U relationship with age, and spatially characterizing a biologically meaningful network of gray matter regions largely involved in transmodal processing. This network of brain regions not only showed mirroring of healthy developmental and aging processes, but also demonstrated heightened vulnerability to etiologically distinct clinical disorders linked to abnormal adolescent and aging trajectories (schizophrenia and Alzheimer's disease) and recapitulated the pattern of macrostructural abnormalities seen in both disorders.

Two features of our methodological approach were crucial in revealing this inverted-U component IC4 showing symmetrical developmental and aging processes. First, no constraint—spatial or age-related—was imposed on the data. Second, the method allowed us to detect more subtle modes of variation over and above other global components that dominate the intersubject variability, such as seen in IC1, and that are typically reported in lifespan studies (16). This decomposition approach thus revealed this IC4 component which, while explaining only a modest amount of the structural variance across all 484 healthy subjects (3%), had a strong relationship with age (as age explained 50% of the IC4 variance) and accounted for a substantial part of the spatial variance of Alzheimer's disease and adolescent-onset schizophrenia patterns of abnormalities (30% and 23%, respectively) (Fig. S2).

These results, intrinsically linking development, aging, and two disorders with very distinct ages of onset of symptoms and neuropathological processes, might seem surprising at first. But they become much more intuitive when taking several considerations into account. First, our network of regions in which development and aging mirror one another includes mainly transmodal regions. The heteromodal cortex (or transmodal cortex when including limbic and paralimbic regions) encompasses the highest synaptic levels of bottom-up processing (17). Because it develops later than the rest of the brain, the transmodal cortex is a strong candidate for showing such retrogenesis or last-in, first-out processes. Second, both Alzheimer's disease and schizophrenia have been linked, separately in the literature, to a selective damage to the heteromodal cortex. Indeed, neuropathological and neuroimaging findings suggest that primary lesions responsible for the classic clinical feature of schizophrenia occur in the phylogenetically recent heteromodal cortex (23, 24). Separately, it has been suggested that the pattern of vulnerability in Alzheimer's disease is distributed specifically following "nodes" distributed within the heteromodal cortex (and showing substantial overlap with the default mode network) (25). Interestingly, a retrogenic neuropathological pattern in terms of neuronal cell loss and

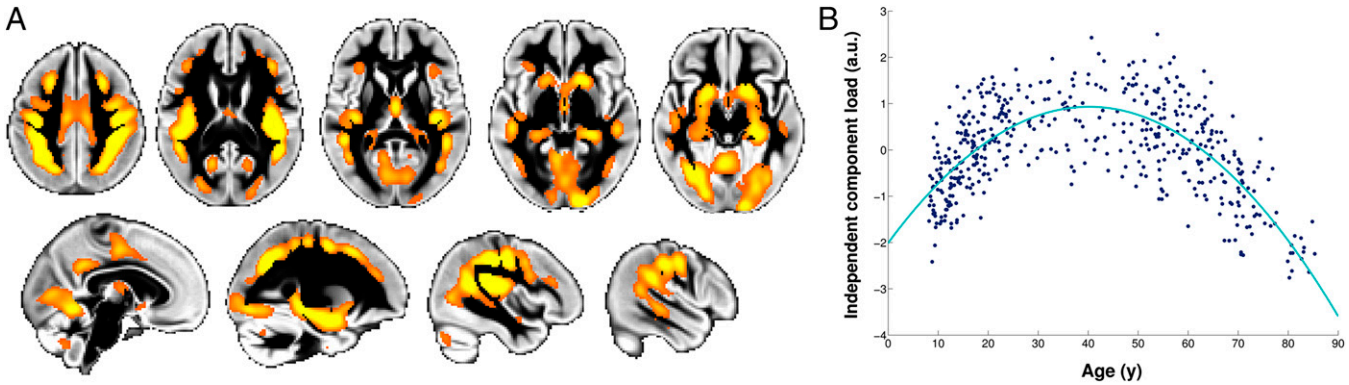

Fig. 2. Network of gray matter regions showing the inverted-U relationship with age. (*A*) Spatial network corresponding to the second age-related independent component IC4 (orange) overlaid on the gray matter average across all 484 healthy participants (thresholded for better visualization at $Z > 4$). Left is right. (*B*) Second age-related independent component IC4 load for each of the 484 participants plotted against age (quadratic fit is in turquoise; $P = 6 \times 10^{-73}$) (*SI Materials and Methods*). a.u., arbitrary unit.

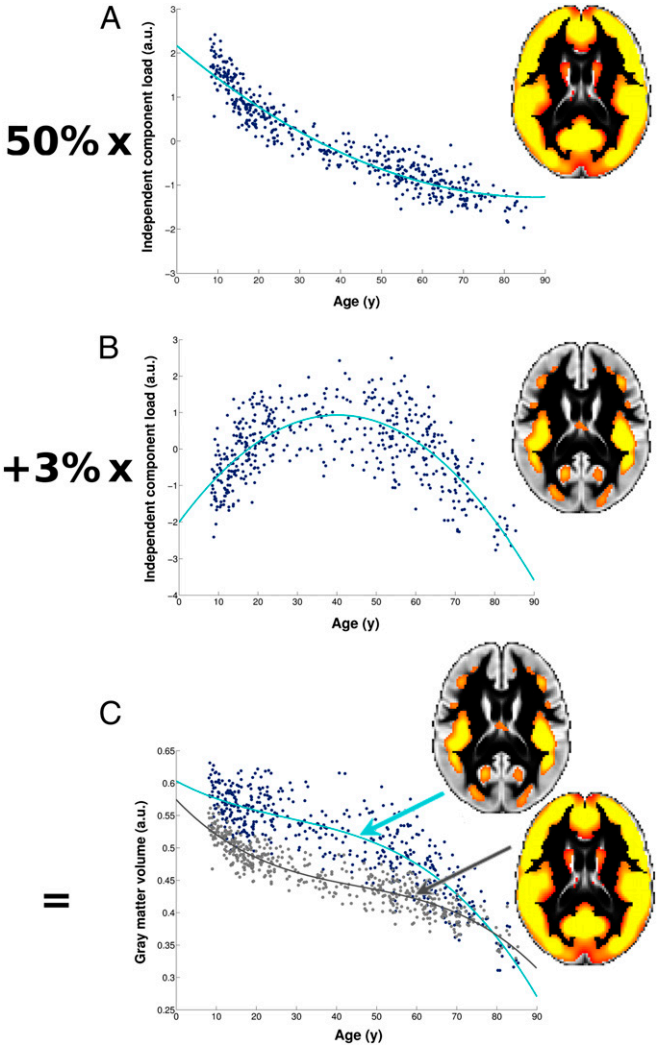

Fig. 3. Regions of the inverted-U network develop relatively slowly during adolescence but present accelerated age-related degeneration at an old age. In the ICA approach, the gray matter volume relationship with age at each voxel is explained by a weighted combination of all ICA components contributing to that voxel. (*A*) A widespread component including most of the gray matter explains 50% of the structural variation in the images (IC1). (*B*) The component of interest (IC4) explains 3% of the structural variation across images. (*C*) The relationship with age in the "core" of the inverted-U network of IC4 (as defined here for visual interpretation by using a threshold of $Z > 4$; *B*) is therefore explained by a combination of *A* and *B*, meaning that there is an additional effect on top of the dominant pattern of monotonic decrease in whole gray matter volume with increasing age as seen in IC1. As a result, compared with the whole of the gray matter (gray line in *C*), regions of the inverted-U network of IC4 (turquoise line in *C*) develop relatively slowly during adolescence and young adulthood (the turquoise line shows a less steep slope than the gray line) but also show accelerated age-related degeneration at old age (the turquoise line shows a steeper slope than the gray line). a.u., arbitrary unit.

myelin vulnerability has also been observed in Alzheimer's disease (7).

Not all regions in the inverted-U spatial network of IC4 were transmodal. However, connectivity of OP1 may predispose it to perform more integrative aspects of somatosensory processing (26), while the crus of the cerebellum is most connected to the heteromodal prefrontal and posterior parietal cortices (27). One region that is known to ontogenetically and phylogenetically develop late, but is absent from our network, is the frontal pole (Brodmann area 10) (28). We did not find any evidence for late maturation in this region whose function is still debated (29, 30), which is in line with findings from the MRI study by Hill et al. (2) elegantly linking high-expanding and slowly maturing cortical regions during evolution and human development. However, the lateral portion of M1, which is not typically thought to develop late or degenerate early, was present in our network, and also within the regions reported in the MRI study by Hill et al. (2). The fact that, using structural MRI, we are probing information at a macroscopic scale, which might encapsulate various cellular mechanisms such as myelination, astrocytosis, or vascularization, might explain these apparent discrepancies. At this resolution, it is not possible to resolve which mechanisms may underlie the macroscopic cortical changes that we observe and peak at 40 y (8). This study also comes with the limitations inherent to large cross-sectional datasets across the lifespan, such as possible cohort effects and selection bias, which might influence the age peak to some degree (31). Various imaging studies support a similar timeline for late development (32–35), however, while recent cellular findings show, for instance, that myelination and remodeling of synaptic spines extend later than previously thought, beyond adolescence and young adulthood (36, 37).

It should be noted that relatively late maturation in the lateral part of the primary motor cortex and small part of lingual gyrus is also seen during healthy adolescence and in adolescent-onset schizophrenia (38, 39). We have previously found that adolescent-onset schizophrenia exhibits an altered maturational pattern compared with matched healthy adolescents (38), with differences in M1, SMA, and lingual gyrus initially present at 16 y, and fading away 2.5 y later. One difference between the inverted-U network of IC4 and the spatial pattern of adolescent-onset schizophrenia was the absence of medial temporal lobe abnormalities in the latter case (Figs. S1 and S3). This apparent discrepancy is likely due to the fact that we observed changes over a relatively short period of time in adolescence (16–18.5 y on average), which did not span to young adulthood when hippocampus volume still changes (40).

Remarkably, the white matter myelination in the frontal lobe, as assessed using diffusion imaging and transverse relaxation rate, reveals a similar inverted-U relationship, peaking at a comparable age (41). It is therefore possible that what we observe here as a subtle effect in the gray matter (on top of the dominating loss of gray matter) relates to the myelination process of intracortical fibers (12). This process might also explain why the spatial distribution of the inverted-U component IC4, and the maps of structural abnormalities in schizophrenia and Alzheimer's disease, is more prominent in the fundus of the sulci as opposed to gyral crowns. Known histological differences between the two, such as the facts that the cortex in the fundus has a greater cell density and, most relevantly, that fundi have thicker supragranular—phylogenetically newest and latest myelinated—layers (42), might partly explain this topography of the gray matter volume differences. Neuropathological studies also interestingly show that β-amyloid distribution in Alzheimer's disease and reduced cell density in schizophrenia are both preferentially found in the fundus of sulci (43, 44). We cannot exclude the possibility, however, that the distinct topography of the cortical fundi and subcortical structures, as more "internal" structures in the brain, and their specific histology and fiber orientation interact with the imaging technique, contrast, and limited resolution used here, so that we are more sensitive to capture macroscopic differences—due to the myelination process, for instance—in these specific parts of the cortex. It is therefore possible that the same brain regions of the inverted-U network might exhibit the same age-related changes in the gyri, if higher-resolution and comparative histology were available (45).

Another feature of the inverted-U component IC4 was that its lifespan trajectory matched that of fluid and crystallized intelligence (that is, before it crystallizes) and, to a lesser degree, episodic memory in the 484 healthy subjects (Fig. S6). As a consequence, there was a linear relationship between the inverted-U component load and each of these cognitive measures, very much in line with the above-mentioned quadratic, inverted-U

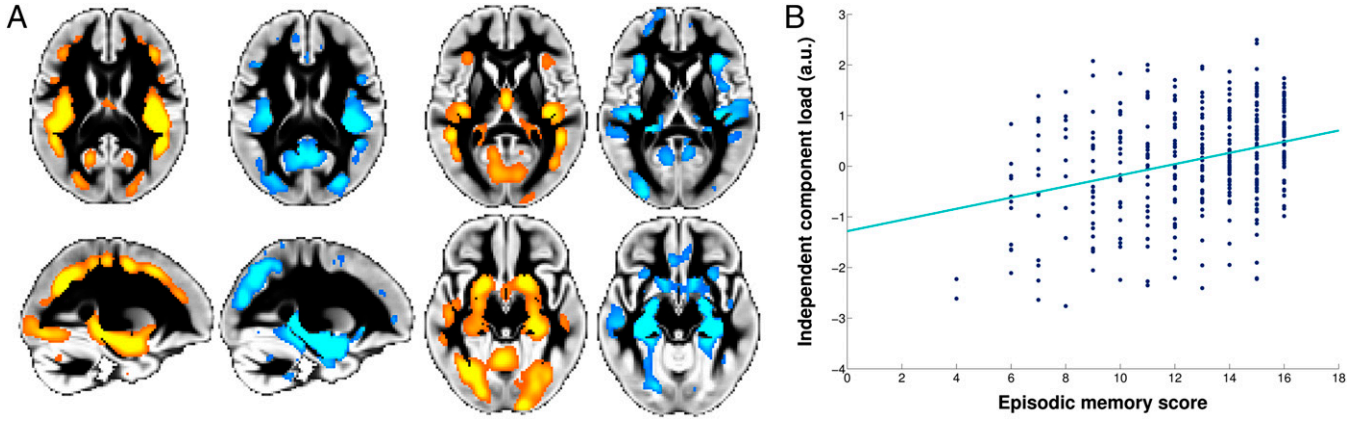

Fig. 4. The inverted-U component spatially corresponds to the structural pattern of abnormalities in Alzheimer's disease and correlates with episodic memory in healthy subjects. (*A*) The spatial network corresponding to the inverted-U component IC4 (orange) closely matches the gray matter found to be atrophic in Alzheimer's disease compared with healthy elderly (blue; thresholded for better visualization at $P < 0.001$; $n = 120$; voxel-by-voxel spatial cross-correlation: $r = 0.55$; $P < 10^{-3}$). (*B*) The inverted-U component load for each of the healthy participants plotted against episodic memory score (CVLT long-delay recall; $n = 370$; linear fit is in turquoise; $r = 0.31$; $P = 1.2 \times 10^{-9}$) (*SI Materials and Methods*). Results presented here have not been age-corrected, as the relationship between episodic memory scores and age was highly nonlinear. In fact, their lifespan trajectory matched that of the inverted-U component (Fig. S6), explaining the linear relationship between the two presented in *B*. a.u., arbitrary unit.

myelination process which followed closely the same age trajectory as a functional performance measure (46). Following these observations, Bartzokis (47) proposed a myelin "development-to-degeneration" model of the human brain, according to which "myelin development, maintenance, and its eventual breakdown are essential to understanding … cognitive and behavioral trajectories through life" and that shed light on Alzheimer's disease as a developmental disorder "requiring myelination as an essential permissive step" (47). This analogous result reinforces the idea, which cannot be tested with the imaging technique and resolution available for this study, that the effect observed here in the gray matter might be somewhat related to myelination.

Using a data-driven approach, we have therefore been able to characterize a biologically meaningful component intrinsically linking late development, early degeneration, and vulnerability to disease. There is mounting evidence that the pattern of various brain disorders can be explained to some extent by observing the healthy brain. Deviations from normal trajectories of brain maturation have been identified in developmental disorders (38, 48), while some neurodegenerative disorders seem to progress within specific healthy brain networks (23, 49). One recent study has also shown that data-driven decomposition of white matter tractograms in healthy young subjects recapitulates the pattern of abnormalities in dementia (50). Here, we show how the symmetric inverted-U component, while derived without any prior hypothesis from healthy subjects' brain structure, (*i*) spatially recapitulates the structural vulnerability of two etiologically distinct disorders emerging at opposite ends of the life spectrum (schizophrenia—aptly named "dementia praecox" until the mid-1950s—and Alzheimer's disease), (*ii*) accurately discriminates these two disorders from their matched healthy group, and (*iii*) is associated, in this large-scale lifespan healthy population, with cognitive functions whose impairment are key symptoms of schizophrenia and Alzheimer's disease. We thus suggest that the

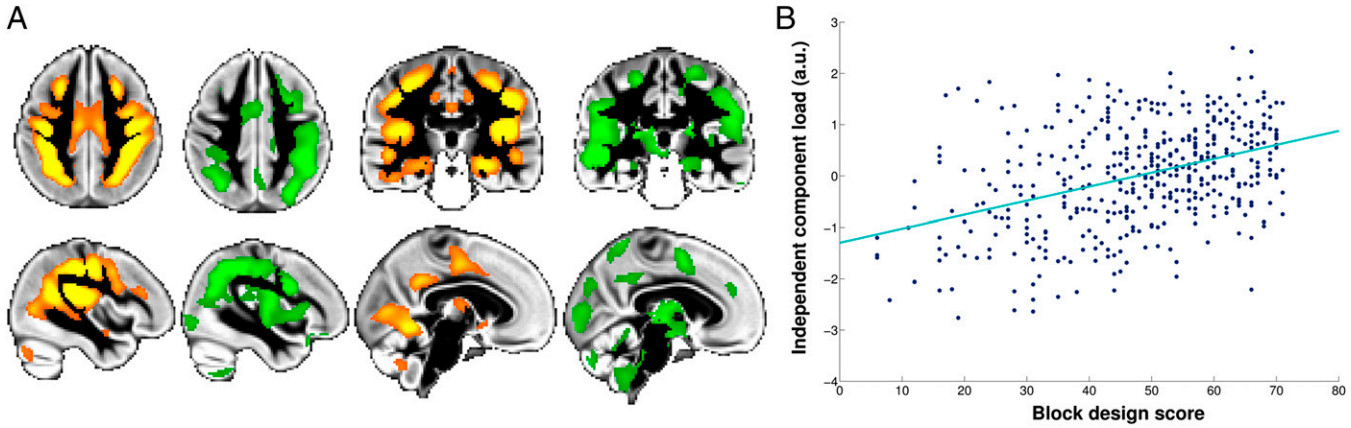

Fig. 5. The inverted-U component spatially corresponds to the structural pattern of abnormalities in adolescent-onset schizophrenia and correlates with intelligence scale in healthy subjects. (*A*) The spatial network corresponding to the inverted-U component IC4 (orange) closely matches the gray matter showing altered trajectory in adolescent-onset schizophrenia compared with healthy adolescents (green; thresholded for better visualization at $P < 0.05$; $n = 24$; voxel-by-voxel spatial cross-correlation: $r = 0.48$; $P < 10^{-3}$). (*B*) The inverted-U component load for each of the healthy participants plotted against intellectual ability [e.g., block design score (fluid intelligence) from the Wechsler Abbreviated Scale of Intelligence; $n = 439$; linear fit is in turquoise; $r = 0.40$; $P = 1.8 \times 10^{-18}$] (*SI Materials and Methods* and Fig. S5 shows the plot for crystallized intelligence). Results presented here have not been age-corrected, as the relationship between block design scores and age was highly nonlinear. As for episodic memory scores, lifespan trajectory of fluid intelligence matched that of the inverted-U component (Fig. S6), explaining the linear relationship between the two presented in *B*. a.u., arbitrary unit.

spatial pattern of structural abnormalities common to these disorders might be determined crucially by the timing of the interplay of their specific pathophysiological processes with normal brain development and aging, specifically in regions in which these two processes mirror one another.

Materials and Methods

The study was approved by the Regional Ethical Committee of Southern Norway; 484 right-handed healthy volunteers covering much of the lifespan (age range from 8 to 85 y old; 220 males) underwent the same imaging protocol with structural T1-weighted images performed using a 12-channel head coil on a 1.5 T Siemens Avanto Scanner (Siemens Medical Systems). A linked ICA decomposition into 70 components was run on brain structural information derived from three complementary types of gray matter image processing: gray matter volume obtained from an optimized voxel-based morphometry protocol using FMRIB Sofware Library (FSL-VBM) analysis (51, 52), and vertexwise cortical thickness and surface area measures calculated using FreeSurfer (53). For the purpose of this study, we focused on components showing statistical as well as clear practical significant relationship with age (significance measured using effect magnitude as opposed to *P* values). We tested for a difference in the peak of the curves between males (n = 224) and females (n = 260) in age and height using bootstrap resampling with replacement. We carried out voxel-by-voxel spatial cross-correlation to quantify the overlap between the spatial map of the age-related independent components and the maps of the structural abnormalities in schizophrenia and Alzheimer's disease, using the values of all voxels within a brain mask. We assessed the significance of the spatial cross-correlation using a Monte Carlo approach. Linear discriminant analysis and leave-one-out cross-validation were carried out in R. Finally, we correlated the strength of the age-related components with the behavioral measures in MATLAB7.12, correcting for multiple comparisons across all components. More details of the method are provided in *SI Materials and Methods*.

ACKNOWLEDGMENTS. We thank Dr. Tom Nichols for his valuable help on statistical questions. We also thank Dr. Peter Keating for helpful comments on this manuscript and further advice on statistical issues. Finally, we thank Prof. André Adoutte for his wonderful and unforgettable lectures in evo-devo. This work was supported by Medical Research Council (MRC) MR/K006673/1 (to G.D.), MRC G0500092 (to A.J.), Research Council of Norway 204966/F20 (to L.T.W.), and Wellcome Trust WT090955AIA (to H.J.-B.). P.M.M. acknowledges research support from the Imperial College Biomedical Research Centre.

1. de Magalhães JP, Church GM (2005) Genomes optimize reproduction: Aging as a consequence of the developmental program. *Physiology (Bethesda)* 20:252–259.
2. Hill J, et al. (2010) Similar patterns of cortical expansion during human development and evolution. *Proc Natl Acad Sci USA* 107(29):13135–13140.
3. Karama S, et al. (2014) Childhood cognitive ability accounts for associations between cognitive ability and brain cortical thickness in old age. *Mol Psychiatry* 19(5):555–559.
4. Tamnes CK, et al.; Alzheimer's Disease Neuroimaging Initiative (2013) Brain development and aging: Overlapping and unique patterns of change. *Neuroimage* 68:63–74.
5. Ribot T (1881) *Les Maladies de la Mcamoire* (Germer-Baillicre, Paris).
6. Raz N, et al. (2005) Regional brain changes in aging healthy adults: General trends, individual differences and modifiers. *Cereb Cortex* 15(11):1676–1689.
7. Reisberg B, et al. (2002) Evidence and mechanisms of retrogenesis in Alzheimer's and other dementias: Management and treatment import. *Am J Alzheimers Dis Other Demen* 17(4):202–212.
8. Zatorre RJ, Fields RD, Johansen-Berg H (2012) Plasticity in gray and white: Neuroimaging changes in brain structure during learning. *Nat Neurosci* 15(4):528–536.
9. Sagi Y, et al. (2012) Learning in the fast lane: New insights into neuroplasticity. *Neuron* 73(6):1195–1203.
10. Sampaio-Baptista C, et al. (2013) Motor skill learning induces changes in white matter microstructure and myelination. *J Neurosci* 33(50):19499–19503.
11. Raz N (2000) Ageing of the brain and its impact on cognitive performance: Integration of structural and functional findings. *Handbook of Aging and Cognition – II*, eds Craik FIM, Salthouse TA (Erlbaum, Mahwah, NJ), pp 1–90.
12. Raz N (2005) *Ageing and the Brain*. Available at onlinelibrary.wiley.com/doi/10.1038/npg.els.0004063/abstract.
13. McGinnis SM, Brickhouse M, Pascual B, Dickerson BC (2011) Age-related changes in the thickness of cortical zones in humans. *Brain Topogr* 24(3-4):279–291.
14. Raz N, Rodrigue KM (2006) Differential aging of the brain: Patterns, cognitive correlates and modifiers. *Neurosci Biobehav Rev* 30(6):730–748.
15. Groves AR, Beckmann CF, Smith SM, Woolrich MW (2011) Linked independent component analysis for multimodal data fusion. *Neuroimage* 54(3):2198–2217.
16. Lemaitre H, et al. (2012) Normal age-related brain morphometric changes: Nonuniformity across cortical thickness, surface area and gray matter volume? *Neurobiol Aging* 33(3):617–619.
17. Mesulam MM (1998) From sensation to cognition. *Brain* 121(Pt 6):1013–1052.
18. Paus T, Keshavan M, Giedd JN (2008) Why do many psychiatric disorders emerge during adolescence? *Nat Rev Neurosci* 9(12):947–957.
19. Fjell AM, et al.; Alzheimer Disease Neuroimaging Initiative (2014) Accelerating cortical thinning: Unique to dementia or universal in aging? *Cereb Cortex* 24(4):919–934.
20. Salem JE, Kring AM (1998) The role of gender differences in the reduction of etiologic heterogeneity in schizophrenia. *Clin Psychol Rev* 18(7):795–819.
21. Bowler JV, Munoz DG, Merskey H, Hachinski V (1998) Factors affecting the age of onset and rate of progression of Alzheimer's disease. *J Neurol Neurosurg Psychiatry* 65(2):184–190.
22. Whitwell JL, et al. (2008) MRI patterns of atrophy associated with progression to AD in amnestic mild cognitive impairment. *Neurology* 70(7):512–520.
23. Buckner RL, et al. (2009) Cortical hubs revealed by intrinsic functional connectivity: Mapping, assessment of stability, and relation to Alzheimer's disease. *J Neurosci* 29(6):1860–1873.
24. Pearlson GD, Petty RG, Ross CA, Tien AY (1996) Schizophrenia: A disease of heteromodal association cortex? *Neuropsychopharmacology* 14(1):1–17.
25. Buckner RL, et al. (2005) Molecular, structural, and functional characterization of Alzheimer's disease: Evidence for a relationship between default activity, amyloid, and memory. *J Neurosci* 25(34):7709–7717.
26. Eickhoff SB, et al. (2010) Anatomical and functional connectivity of cytoarchitectonic areas within the human parietal operculum. *J Neurosci* 30(18):6409–6421.
27. O'Reilly JX, Beckmann CF, Tomassini V, Ramnani N, Johansen-Berg H (2010) Distinct and overlapping functional zones in the cerebellum defined by resting state functional connectivity. *Cereb Cortex* 20(4):953–965.
28. Semendeferi K, Armstrong E, Schleicher A, Zilles K, Van Hoesen GW (2001) Prefrontal cortex in humans and apes: A comparative study of area 10. *Am J Phys Anthropol* 114(3):224–241.
29. Ramnani N, Owen AM (2004) Anterior prefrontal cortex: Insights into function from anatomy and neuroimaging. *Nat Rev Neurosci* 5(3):184–194.
30. Koechlin E, Hyafil A (2007) Anterior prefrontal function and the limits of human decision-making. *Science* 318(5850):594–598.
31. Fjell AM, et al.; Alzheimer Disease Neuroimaging Initiative (2013) Critical ages in the life course of the adult brain: Nonlinear subcortical aging. *Neurobiol Aging* 34(10):2239–2247.
32. Lebel C, et al. (2012) Diffusion tensor imaging of white matter tract evolution over the lifespan. *Neuroimage* 60(1):340–352.
33. Westlye LT, et al. (2010) Life-span changes of the human brain white matter: Diffusion tensor imaging (DTI) and volumetry. *Cereb Cortex* 20(9):2055–2068.
34. Kochunov P, et al. (2011) Fractional anisotropy of cerebral white matter and thickness of cortical gray matter across the lifespan. *Neuroimage* 58(1):41–49.
35. Grydeland H, Walhovd KB, Tamnes CK, Westlye LT, Fjell AM (2013) Intracortical myelin links with performance variability across the human lifespan: Results from T1- and T2-weighted MRI myelin mapping and diffusion tensor imaging. *J Neurosci* 33(47):18618–18630.
36. Miller DJ, et al. (2012) Prolonged myelination in human neocortical evolution. *Proc Natl Acad Sci USA* 109(41):16480–16485.
37. Petanjek Z, et al. (2011) Extraordinary neoteny of synaptic spines in the human prefrontal cortex. *Proc Natl Acad Sci USA* 108(32):13281–13286.
38. Douaud G, et al. (2009) Schizophrenia delays and alters maturation of the brain in adolescence. *Brain* 132(Pt 9):2437–2448.
39. Westlye LT, et al. (2010) Differentiating maturational and aging-related changes of the cerebral cortex by use of thickness and signal intensity. *Neuroimage* 52(1):172–185.
40. Hedden T, Gabrieli JD (2004) Insights into the ageing mind: A view from cognitive neuroscience. *Nat Rev Neurosci* 5(2):87–96.
41. Bartzokis G, et al. (2012) Multimodal magnetic resonance imaging assessment of white matter aging trajectories over the lifespan of healthy individuals. *Biol Psychiatry* 72(12):1026–1034.
42. Clinton J, Roberts GW, Gentleman SM, Royston MC (1993) Differential pattern of beta-amyloid protein deposition within cortical sulci and gyri in Alzheimer's disease. *Neuropathol Appl Neurobiol* 19(3):277–281.
43. Chance SA, Tzotzoli PM, Vitelli A, Esiri MM, Crow TJ (2004) The cytoarchitecture of sulcal folding in Heschl's sulcus and the temporal cortex in the normal brain and schizophrenia: Lamina thickness and cell density. *Neurosci Lett* 367(3):384–388.
44. Gentleman SM, et al. (1992) Quantitative differences in the deposition of beta A4 protein in the sulci and gyri of frontal and temporal isocortex in Alzheimer's disease. *Neurosci Lett* 136(1):27–30.
45. Budde MD Annese J (2013) Quantification of anisotropy and fiber orientation in human brain histological sections. *Front Integrative Neurosci* 7(2013):3.
46. Bartzokis G, et al. (2010) Lifespan trajectory of myelin integrity and maximum motor speed. *Neurobiol Aging* 31(9):1554–1562.
47. Bartzokis G (2011) Alzheimer's disease as homeostatic responses to age-related myelin breakdown. *Neurobiol Aging* 32(8):1341–1371.
48. Shaw P, et al. (2007) Attention-deficit/hyperactivity disorder is characterized by a delay in cortical maturation. *Proc Natl Acad Sci USA* 104(49):19649–19654.
49. Seeley WW, Crawford RK, Zhou J, Miller BL, Greicius MD (2009) Neurodegenerative diseases target large-scale human brain networks. *Neuron* 62(1):42–52.
50. Raj A, Kuceyeski A, Weiner M (2012) A network diffusion model of disease progression in dementia. *Neuron* 73(6):1204–1215.
51. Douaud G, et al. (2007) Anatomically related grey and white matter abnormalities in adolescent-onset schizophrenia. *Brain* 130(Pt 9):2375–2386.
52. Smith SM, et al. (2004) Advances in functional and structural MR image analysis and implementation as FSL. *Neuroimage* 23(Suppl 1):S208–S219.
53. Fischl B, et al. (2002) Whole brain segmentation: Automated labeling of neuroanatomical structures in the human brain. *Neuron* 33(3):341–355.

Supporting Information

Douaud et al. 10.1073/pnas.1410378111

SI Materials and Methods

1. Linked ICA.

Participants. In total, 484 right-handed healthy volunteers covering much of the lifespan (age range from 8 to 85 y old; 220 males) were selected from two research projects run by the Research Group for Lifespan Changes in Brain and Cognition at the University of Oslo ("Neurocognitive Development" and "Cognition and Plasticity through the Lifespan"). The study was approved by the Regional Ethical Committee of Southern Norway.

The majority of participants was recruited through newspaper advertisements. Written informed consent was obtained from all participants ≥ 12 y of age and from parents for participants < 18 y of age. Oral informed consent was given by participants < 12 y of age. All subjects were fluent Norwegian speakers and screened using a standardized health interview before inclusion in the study. Exclusion criteria comprised history of self- or parent-reported neurological or psychiatric conditions including stroke, head injury, untreated hypertension, diabetes, use of psychoactive drugs within the last 2 y, and concerns with cognitive status—including memory function. All included MRI scans were examined by a neuroradiologist and deemed free of significant anomalies, including brain tumors and significant vascular insults (stroke).

Imaging acquisition. All participants underwent the same imaging protocol performed using a 12-channel head coil on a 1.5 T Siemens Avanto Scanner (Siemens Medical Solutions) at Oslo University Hospital, Rikshospitalet, with no hardware upgrades and only minor software upgrades performed during the course of the acquisition period (2006–2010). Whole-brain T1-weighted images were acquired using magnetization prepared rapid gradient echo (MPRAGE) with the following parameters: repetition time/echo time/inversion time (TR/TE/TI) = 2,400/3.61/1,000 ms, flip angle of 8°, matrix = 192 × 192, field of view = 240 mm, voxel size of 1.25 × 1.25 × 1.2 mm^3, and 160 sagittal slices. To increase signal-to-noise ratio, the sequence was repeated twice within a single session.

Imaging processing. T1-weighted images were processed using FSL-VBM (1), an optimized voxel-based morphometry protocol (2) using FMRIB Software Library (FSL) tools (3), in which a symmetric study-specific gray matter (GM) template was built from all of the participants' images (fsl.fmrib.ox.ac.uk/fsl/fslwiki/FSLVBM; FSL 4.1.7). For each subject, the input image for FSL-VBM was an average of two repeated MPRAGE sequences. Briefly, the two runs were preprocessed using FreeSurfer, including motion correction, averaging, and intensity nonuniformity correction. Prior to the FSL-VBM processing, the volumes were masked by the full brain-segmented volume output from FreeSurfer (surfer.nmr.mgh.harvard.edu; FreeSurfer 5.0.0) (4), effectively excluding nonbrain compartments. After nonlinearly registering all of the brain-extracted, GM-segmented images onto the symmetric study-specific GM template, the optimized FSL-VBM protocol involved a compensation (or "modulation") for the local contraction/enlargement caused by the nonlinear component of the transformation: each voxel of each registered GM image was multiplied by the Jacobian of the warp field. The modulated registered GM-segmented images were then smoothed with an isotropic Gaussian kernel with a σ of 4 mm (~9.4 mm full width at half maximum).

In addition, brain structural information was also derived from two other complementary types of GM image processing: vertexwise cortical thickness and surface area measures calculated using FreeSurfer by means of an automated surface reconstruction scheme (4).

Linked ICA. Linked ICA is an entirely data-driven approach that can comodel multiple imaging modalities. Its main goal is to model the imaging data as a set of interpretable features (independent components), most of them characterizing biophysically plausible modes of variability across all subjects' images. Unlike in a principal component analysis, the mixing matrix vectors of an ICA are not forced to be orthogonal to each other, and thus can explain common variance of variables external to the ICA, such as age. Linked ICA is implemented as described in detail in earlier papers (5, 6) (http://fsl.fmrib.ox.ac.uk/fsl/fslwiki/FLICA). We ran the linked ICA decomposition with 70 components to make it comparable with the work by Smith et al. (7). Linked ICA is capable of eliminating unneeded components (using Bayesian model order selection), but in all cases here, it kept all components.

2. Components Showing Relationship with Age. For the purpose of this study, we focused on components showing relationship with age (as assessed using a quadratic fit). There were eight such components, but only two achieved statistical as well as clear practical significance: IC1 and IC4 (significance measured using effect magnitude as opposed to P values) (Fig. 1) (8). The first such component (IC1) was the expected global dominant mode showing monotonic decrease of the whole GM with age (except for the medial temporal lobe). The weight for this IC1 component was essentially composed of GM volume information (42%) and cortical thickness (51%), and only very modestly of cortical area (7%). In contrast, the other component (IC4) showed a nonmonotonic relationship with age, describing a symmetric inverted-U shape with age with the strongest quadratic coefficient of all age-related components. The weight for this IC4 component was largely carried by GM volume information (53%) rather than thickness (20%) or area (23%), and the latter two contributions did not survive a threshold of $Z > 4$. In the opposite contrast (i.e., decreasing in early age and increasing in older age), cortical thickness showed a strong effect in the anterior and ventral medial cingulate cortex and the insula (nonoverlapping with volume effects) and volume effects in the inferior temporal gyrus. This somewhat surprising result is actually in line with what Salat et al. (9, 10) have consistently observed with aging in the anterior cingulate cortex and the inferior temporal gyrus, and might be related to a change in intensity and contrast in these specific brain areas, for which the histological mechanism are unclear.

The best fit for the relationship between this second component IC4 and age was quadratic ($P = 6 \times 10^{-73}$) in the shape of an inverted U with a peak at 40.2 y: $y = -0.00182x^2 + 0.14643x - 2.00964$ (norm of residuals = 15.57; goodness of fit: sum of squared errors (SSE) = 242.5; adjusted $R^2 = 0.50$; MATLAB7.12). A cubic fit showed no substantial improvement (norm of residuals = 15.53). Quadratic models also provided a good fit for the relationship between the second age-related component IC4 and age for males and females taken separately (Fig. S4). We tested for a difference in the peak of the curves between males ($n = 224$) and females ($n = 260$) in age and height using bootstrap resampling with replacement: we computed this difference based on separate quadratic fits for two populations of same size ($n = 224$ and $n = 260$), both of them randomly sampled from the entire healthy population of $n = 484$ (10,000 iterations). The peak of the curve was significantly higher and later for females than males at 40.9 y for females compared with 38.8 y for males ($P < 10^{-4}$ and $P = 4.5 \times 10^{-3}$, respectively).

There was a nonmonotonic inverted-U relationship between the two age-related components IC1 and IC4 that was fully driven

by their strong relationships to age (as age explained 90% of the variance of the dominant age-related component IC1 and 50% of the variance of the second age-related component IC4); when the modeled age-quadratic effect was removed from both components, their residuals showed no relationship.

3. Comparison with Alzheimer's Disease and Adolescent-Onset Schizophrenia.

Participants. The Alzheimer's disease (AD) cohort comprised 62 healthy controls and 58 AD patients (overall mean age = 73 ± 8 y). Subjects' demographics, and inclusion/exclusion and diagnosis criteria, have been previously described (11). The 120 participants underwent the same imaging protocol on a 3 T Allegra MR Imager (Siemens) with a standard quadrature head coil and maximum 40 $mT.m^{-1}$ gradient capability. This imaging protocol included whole-brain T1-weighted scanning using MPRAGE with the following parameters: TR/TE/TI = 2,150/3.49/1,000 ms, flip angle of 7°, field of view = 280 mm, voxel size of 1.1 mm isotropic, and 144 sagittal slices. Structural scans were processed using the optimized FSL-VBM protocol (smoothing with 3-mm σ-Gaussian kernel) (1), and *t* maps representing group differences between patients and controls were generated.

For the adolescent-onset schizophrenia (AOS) comparison included here, 12 healthy controls and 12 AOS patients were considered (mean age at baseline = 16.0 ± 1.5 y). Subjects' demographics, inclusion/exclusion criteria, medication, imaging protocol, and results have been previously described in detail (12). Structural scans at baseline and a second time point (2.5 y later) were reprocessed using the same FSL-VBM protocol as for the 484 healthy participants and the 120 subjects of the AD study (1). The modulated registered GM images from the second time point were subtracted from those at baseline, and the resulting images were smoothed with an isotropic Gaussian kernel with a σ of 4 mm, and *t* maps representing between-group (patients vs. controls) differences in these changes over time were generated.

Spatial cross-correlation. We compared the spatial distribution of the inverted-U component IC4 and the pattern of abnormalities in AD and AOS using voxel-by-voxel spatial cross-correlation in FSL 5.0.5 (3). For this analysis, we first used a nonlinear registration from the average GM map across all 120 elderly participants of the AD cohort onto the average GM map across all 484 healthy participants and applied the warpfield to the map of structural abnormalities in AD. We carried out the same procedure for the AOS cohort. The reason for this step is that, although all images are in the Montreal Neurological Institute (MNI) space, each cohort will be in its own study-specific standard space, as is required by the optimized VBM protocol. As a consequence, the standard space template for the AOS cohort will, for instance, display much smaller ventricles than the one for the AD cohort. Then, we masked each map with the MNI152 brain mask and correlated all voxels of the inverted-U component ($Z > 0$) with the statistical map of regions showing lower volume in AD compared with their matched controls ($t > 0$), and those regions showing late development in AOS compared with matched healthy adolescents ($t > 0$).

To assess the significance of the spatial cross-correlation between the spatial distribution of the inverted-U component IC4 and maps of both AD and AOS structural abnormalities, we randomly generated 1,000 Gaussian noise images that we smoothed with the corresponding estimated smoothness for AD and AOS differences with their respective controls. We then calculated the 1,000 cross-correlations between each of these noise maps and the network corresponding to the inverted-U component and compared the strength of our observed correlations with this empirically generated null distribution.

Prediction of AOS and AD. We spatially regressed the GM network corresponding to the inverted-U component IC4 ($Z > 0$) into the GM volume images of each AD patient and matched control, as well as each AOS patient and matched control. We then used this single measure for each subject to calculate the specificity, sensitivity, and accuracy of prediction of the two clinical disorders using a linear discriminant analysis and leave-one-out cross-validation in datamind (R) (13).

Post hoc correlation with cognitive measures in healthy subjects. Finally, we wanted to investigate post hoc the relationship between the strength of the inverted-U component IC4 and two cognitive measures that are hallmarks of AD and AOS: episodic memory (as assessed with the CVLT long-delay free recall) and the performance (fluid) and verbal (crystallized) intelligence raw scores (block design and vocabulary; WASI) (Figs. 4 and 5). For verbal (crystallized) intelligence, which is known to plateau, we also considered only values for the 249 of 484 healthy participants who were under 40 y old, the peak age for the inverted-U component (Fig. S5). We further assessed if any of these measures still correlated significantly with the inverted-U component strength after regressing out the linear and quadratic effect of age using the linear model in R. All of the correlations survived correction for multiple comparisons across all components and were still significant after correction for linear effect of age, but not for a quadratic effect of age, as lifespan trajectories for fluid intelligence, episodic memory, and inverted-U component were very similar (Fig. S6). For completeness, we compared the correlation values between these cognitive measures and all age-related components (Fig. S2).

1. Douaud G, et al. (2007) Anatomically related grey and white matter abnormalities in adolescent-onset schizophrenia. *Brain* 130(Pt 9):2375–2386.
2. Ashburner J, Friston KJ (2000) Voxel-based morphometry—the methods. *Neuroimage* 11(6 Pt 1):805–821.
3. Smith SM, et al. (2004) Advances in functional and structural MR image analysis and implementation as FSL. *Neuroimage* 23(Suppl 1):S208–S219.
4. Fischl B, et al. (2002) Whole brain segmentation: Automated labeling of neuroanatomical structures in the human brain. *Neuron* 33(3):341–355.
5. Groves AR, Beckmann CF, Smith SM, Woolrich MW (2011) Linked independent component analysis for multimodal data fusion. *Neuroimage* 54(3):2198–2217.
6. Groves AR, et al. (2012) Benefits of multi-modal fusion analysis on a large-scale dataset: Life-span patterns of inter-subject variability in cortical morphometry and white matter microstructure. *Neuroimage* 63(1):365–380.
7. Smith SM, et al. (2009) Correspondence of the brain's functional architecture during activation and rest. *Proc Natl Acad Sci USA* 106(31):13040–13045.
8. Kirk RE (1996) Practical significance: A concept whose time has come. *Educ Psychol Meas* 56(5):746–759.
9. Salat DH, et al. (2004) Thinning of the cerebral cortex in aging. *Cereb Cortex* 14(7):721–730.
10. Salat DH, et al. (2009) Age-associated alterations in cortical gray and white matter signal intensity and gray to white matter contrast. *Neuroimage* 48(1):21–28.
11. Douaud G, et al. (2011) DTI measures in crossing-fibre areas: Increased diffusion anisotropy reveals early white matter alteration in MCI and mild Alzheimer's disease. *Neuroimage* 55(3):880–890.
12. Douaud G, et al. (2009) Schizophrenia delays and alters maturation of the brain in adolescence. *Brain* 132(Pt 9):2437–2448.
13. Duchesnay E, et al. (2007) Classification based on cortical folding patterns. *IEEE Transactions on Medical Imaging* 26(4):553–565.

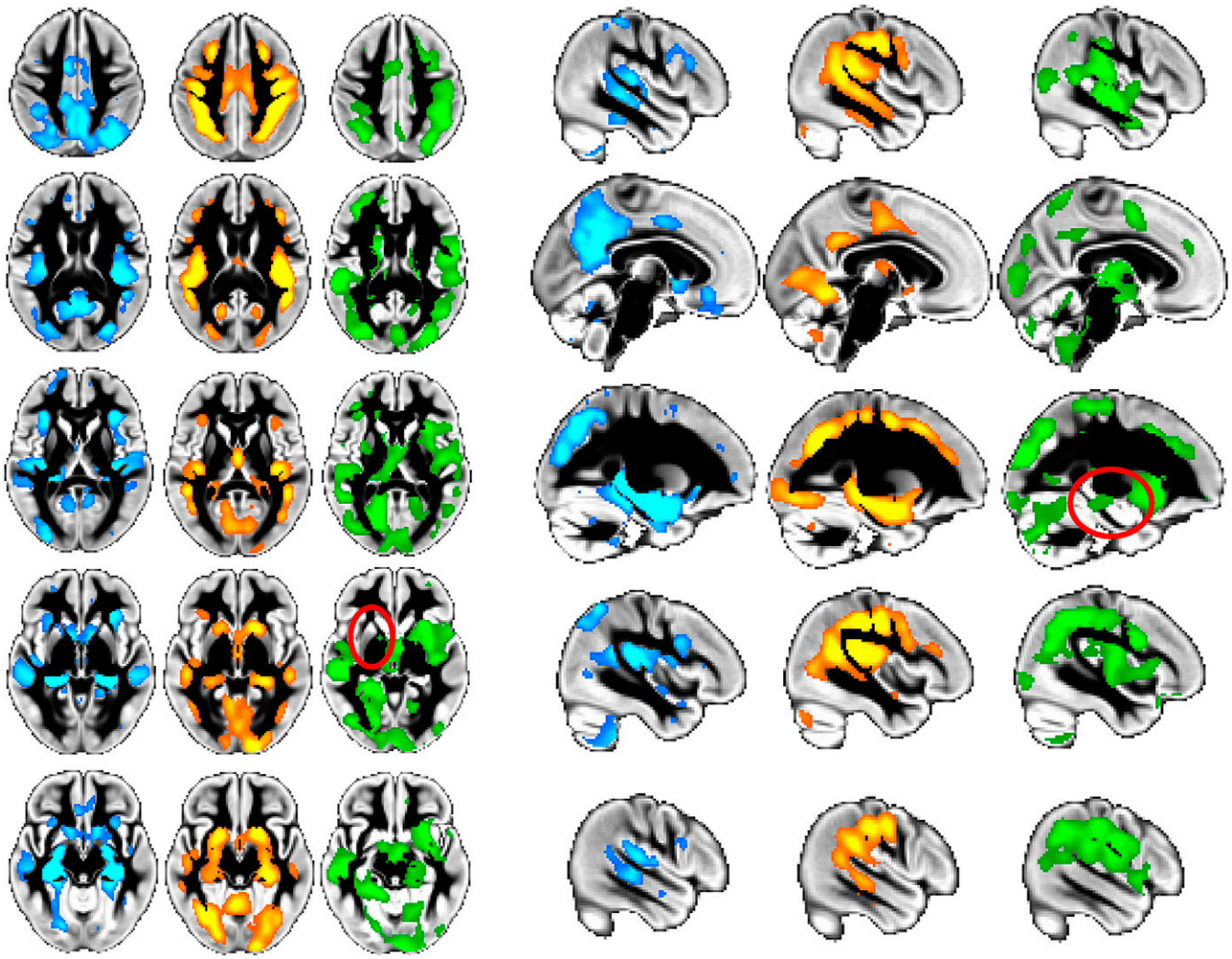

Fig. S1. AD-related abnormalities, the spatial network of the inverted-U component, and AOS-related abnormalities spatially correspond to one another. (*Left*) Axial and (*Right*) sagittal slices showing AD-related abnormalities (blue; thresholded for better visualization at $P < 0.001$), the spatial network of the inverted-U component IC4 (orange; $Z > 4$), and AOS-related abnormalities (green; $P < 0.05$). Main differences are the lack of extensive structural abnormalities in the medial temporal lobe as well as some apparent asymmetry in AOS (red ovals).

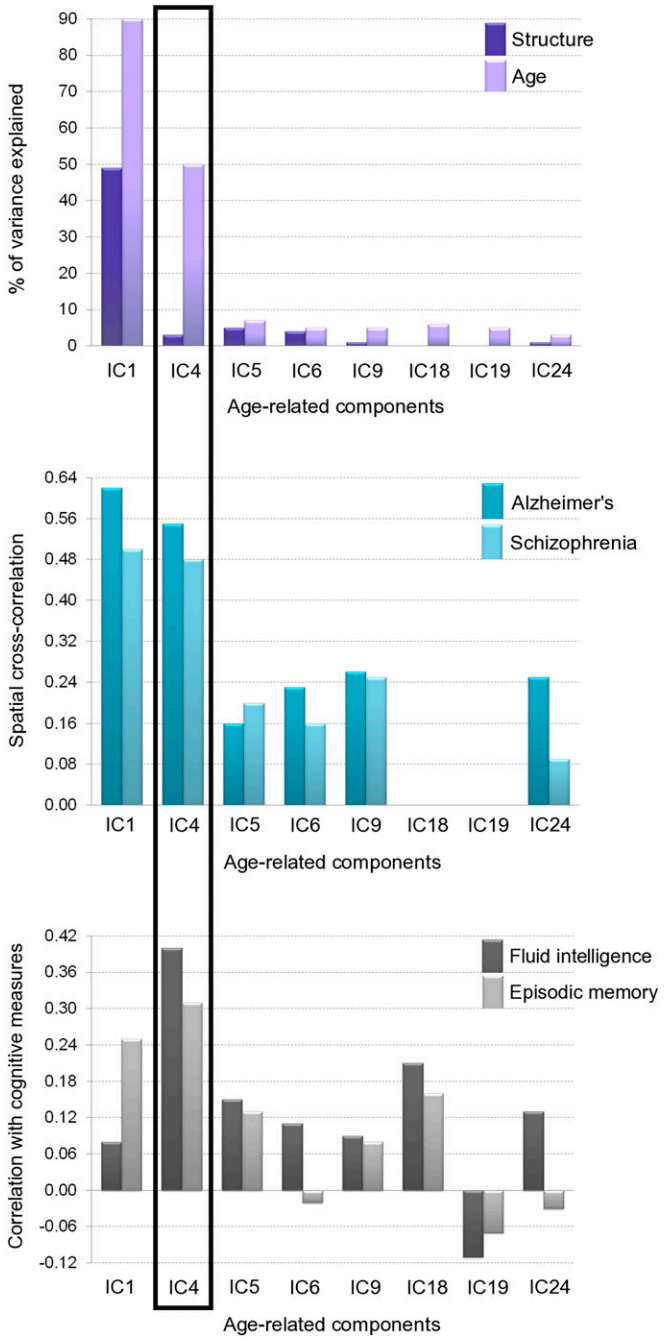

Fig. S2. Characteristics of age-related components. (*Top*) For each of eight components that were significantly related to age (quadratic fit), we measured across all 484 healthy subjects (*i*) the percentage of variance of GM volume ("structure") that the component explained and (*ii*) the percentage of variance within that component explained by age (Fig. 1). Of note, although the inverted-U component (IC4) accounted for only 3% of the variance of GM volume (structure), 50% of the variance within the IC4 component was associated with age. (*Middle*) Spatial cross-correlations between the GM volume map for each age-related component and AD/AOS structural abnormalities: both IC1 (the global component mostly representing the standard deviation of GM volume across all of the subjects) and IC4 (the age-related inverted-U component mostly representing transmodal areas) were highly correlated with AD and AOS spatial distribution of abnormalities. (*Bottom*) Correlations with fluid intelligence (block design; not age-corrected) and episodic memory (CVLT long-delay recall; not age-corrected); across the lifespan and all healthy participants, IC4 had the strongest correlations with both cognitive measures.

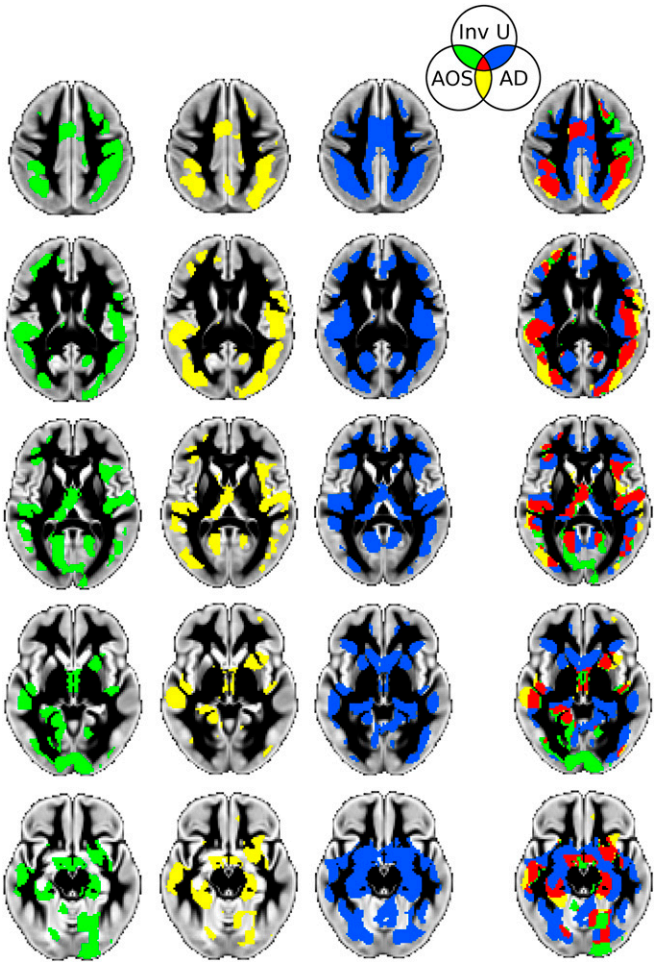

Fig. S3. Binary overlaps show spatial commonality between the pattern of the inverted-U component and the pattern of abnormalities in AD and AOS. In green is the overlap between the inverted-U component IC4 and AOS, in yellow is the "disease" overlap between AD and AOS, and in blue is the overlap between the inverted-U component IC4 and AD (arbitrary threshold at $P < 0.05$). In red is the overlap between all three patterns. The most notable differences are the lack of extensive abnormalities in the amygdalo-hippocampal complex in AOS (see also the main text). Inv U, inverted-U.

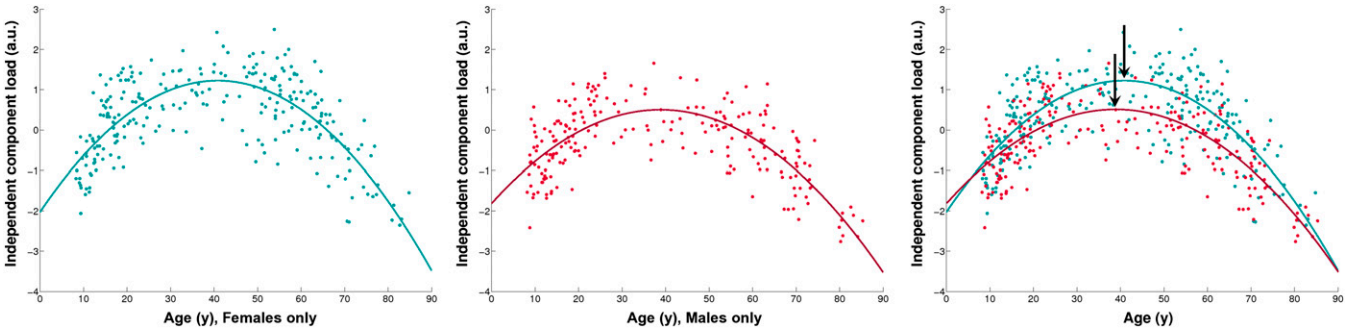

Fig. S4. Inverted-U component load differs between females and males. (*Left*) Inverted-U component IC4 load for all females (turquoise; $n = 260$) and (*Center*) all males (magenta; $n = 224$) plotted against age. (*Right*) A quadratic model provided an excellent fit for the relationship between the component load and age for females ($P = 3.5 \times 10^{-44}$) and males ($P = 1.3 \times 10^{-33}$) taken separately, with a higher, slightly later peak for the females than for the males (black arrows; $P = 4.5 \times 10^{-3}$): females $y_F = -0.00195x_F^2 + 0.15919x_F - 2.0271$; males $y_M = -0.00154x_M^2 + 0.11936x_M - 1.8158$. a.u., arbitrary unit.

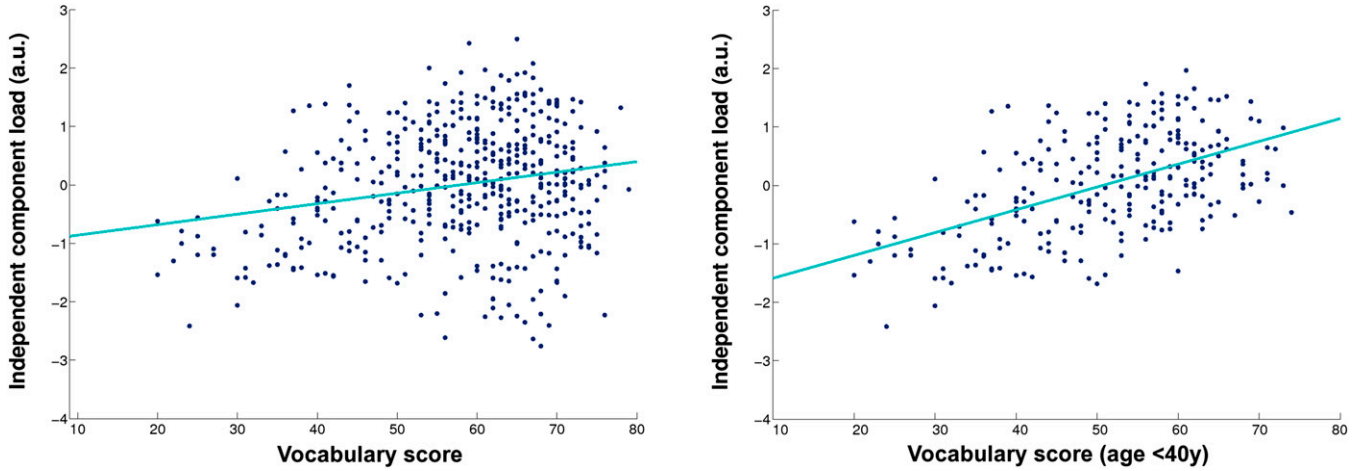

Fig. S5. Inverted-U component load correlates with crystallized intelligence scores in healthy subjects. Crystallized intelligence, in contrast to episodic memory and fluid intelligence, does not peak with age, but instead reaches a plateau. Estimates for this age plateau vary depending on whether they are made, for instance, from cross-sectional or longitudinal data (similar to what has been observed for age peaks in fluid intelligence and episodic memory) (1–3), usually from 25–35 to 45–55 y. We therefore looked at the correlation between the inverted-U component IC4 load and one measure of crystallized intelligence (vocabulary; WASI) not only across all participants, but also for participants under 40 y old, which corresponds to the peak of the inverted U. (*Left*) For all healthy participants ($n = 481$; $r = 0.21$; $P = 2.6 \times 10^{-6}$). (*Right*) Stronger correlation was seen for all healthy participants under 40 y old ($n = 249$; $r = 0.52$; $P = 4.9 \times 10^{-19}$). a.u., arbitrary unit.

1. Rönnlund M, Nyberg L, Bäckman L, Nilsson LG (2005) Stability, growth, and decline in adult life span development of declarative memory: Cross-sectional and longitudinal data from a population-based study. *Psychol Aging* 20(1):3–18.
2. Ronnlund M, Nilsson LG (2006) Adult life-span patterns in WAIS-R Block Design performance: Cross-sectional versus longitudinal age gradients and relations to demographic factors. *Intelligence* 34(1):63–78.
3. Craik FI, Bialystok E (2006) Cognition through the lifespan: Mechanisms of change. *Trends Cogn Sci* 10(3):131–138.

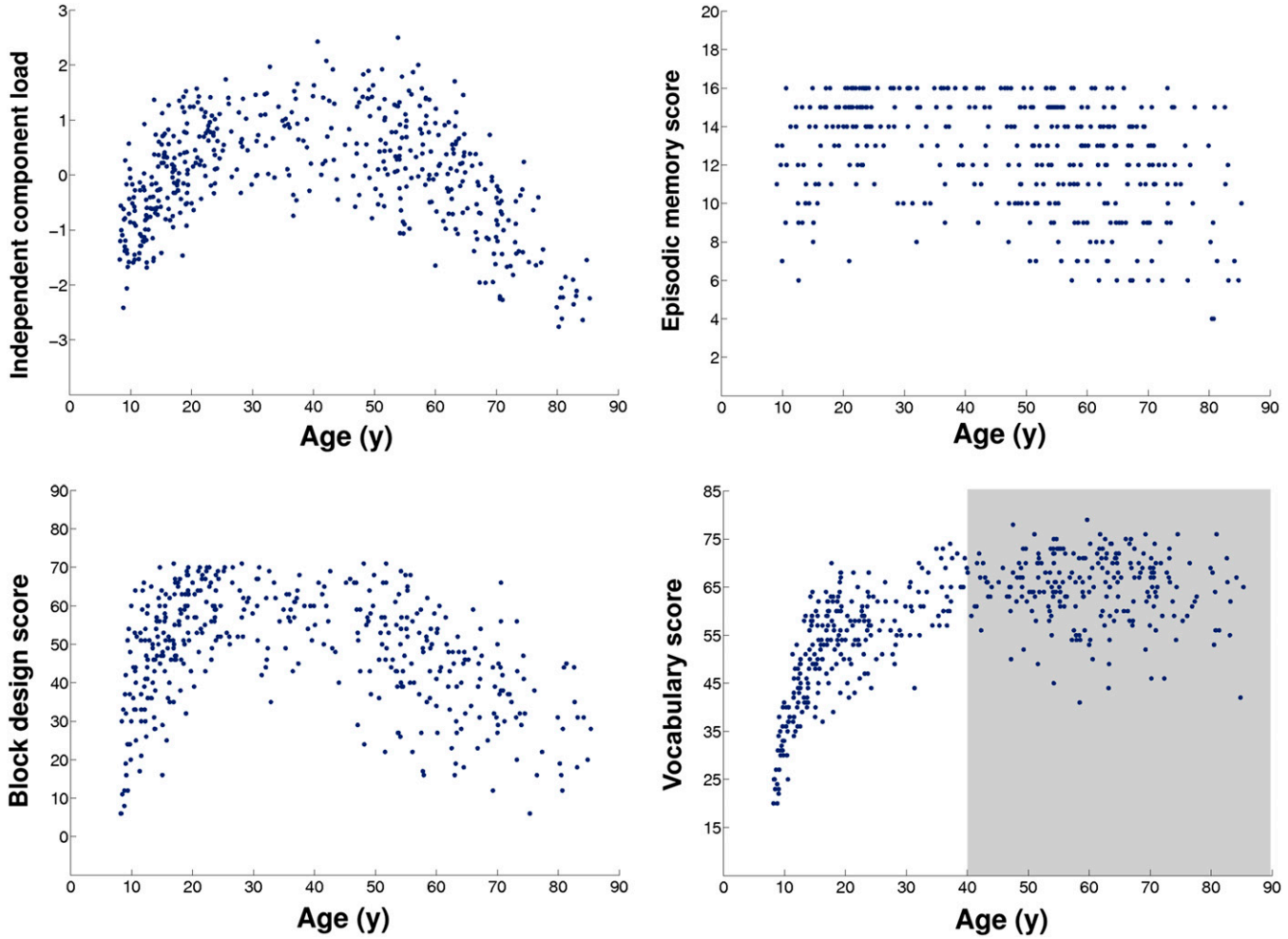

Fig. S6. Similar lifespan trajectories for the inverted-U component, long-term memory, and fluid and crystallized intelligence (<40 y). There were similar inverted-U quadratic relationships between age and inverted-U component IC4 (peaking at 40 y), episodic memory scores (peaking at 32 y), and block design scores (peaking at 38 y). Age trajectory of vocabulary scores before 40 y (when it crystallizes to a plateau) also matched that of the inverted-U component for the same age range (Fig. S5).

Table S1. MNI coordinates of local maxima for the GM network corresponding to the inverted-U component ($Z > 4$)

Cortical region [Brodmann Area (BA)]	Side	MNI (voxel)			*Z* value
		x	*y*	*z*	
Medial temporal areas					
Amygdalohippocampal complex	Left	59	62	26	8.74
Amygdalohippocampal complex	Right	32	61	27	8.91
Dentate gyrus	Left	58	47	32	8.04
Other temporal areas					
Posterior superior temporal sulcus	Left	69	48	35	6.24
Posterior superior temporal sulcus	Right	21	48	35	6.66
Temporoparietal areas					
Supramarginal/angular gyrus	Left	68	39	44	9.78
Supramarginal/angular gyrus	Right	21	41	42	8.17
Parietal areas					
Intraparietal sulcus (anterior)	Right	28	38	56	13.89
Intraparietal sulcus (anterior)	Left	64	46	57	12.12
Intraparietal sulcus (posterior)	Left	58	31	54	12.12
Intraparietal sulcus (posterior)	Right	32	31	54	10.33
Other parietal areas					
Posterior cingulate cortex	Right	40	40	53	7.73
Posterior cingulate cortex	Left	50	39	53	7.56
Parieto-occipital fissure (precuneus)	Left	53	29	51	8.68
Parieto-occipital fissure (precuneus)	Right	37	29	49	8.16
Opercular/insular areas					
Parietal operculum	Left	65	50	44	13.45
Parietal operculum	Right	26	53	44	9.17
Frontal operculum/anterior insula	Right	28	77	38	5.10
Prefrontal areas					
Middle frontal gyrus (BA9)	Right	26	67	52	10.28
Middle frontal gyrus (BA9)	Left	64	66	52	9.19
Middle frontal gyrus (BA46)	Left	65	77	46	6.56
Middle frontal gyrus (BA46)	Right	25	78	45	4.99
Superior frontal gyrus (BA8)	Right	33	71	59	7.47
Superior frontal gyrus (BA8)	Left	57	72	58	7.54
Superior frontal gyrus (BA6)	Right	32	60	61	8.32
Superior frontal gyrus (BA6)	Left	59	60	60	7.93
Medial superior frontal gyrus (BA6)	—	45	57	62	6.44
Other frontal areas					
Precentral gyrus (BA4)	Left	65	55	58	9.85
Precentral gyrus (BA4)	Right	26	54	58	9.46
Occipital areas					
Calcarine fissure	Left	52	14	34	9.24
Lateral occipital cortex	Left	66	30	38	6.57
Lateral occipital cortex	Right	23	33	36	5.03
Lingual gyrus	—	45	24	37	6.62
Lingual gyrus	Right	40	34	38	6.17
Temporo-occipital areas					
Fusiform gyrus	Right	28	30	29	9.12
Fusiform gyrus	Left	61	30	30	5.72
Cerebellum					
Crus I	Right	23	25	21	5.15
Crus I	Left	67	25	21	4.14
I–IV	—	43	35	32	7.85
Subcortical areas					
Ventral striatum	Left	54	69	33	9.79
Ventral striatum	Right	35	68	32	9.18
Thalamus	—	45	57	41	7.79

Regions were identified based on the Harvard–Oxford in vivo probabilistic atlas, the Jülich cytoarchitectonic probabilistic atlas, and the probabilistic cerebellar atlas available in FSL.